

Enable Fully Customized Assistance: A Novel IMU-based Motor Intent Decoding Scheme

Journal:	<i>IEEE Transactions on Cognitive and Developmental Systems</i>
Manuscript ID	TCDS-2020-0402.R2
Manuscript Type:	SI: Trustworthy Autonomous Systems
Date Submitted by the Author:	28-Oct-2021
Complete List of Authors:	Yi, Chunzhi; Harbin Institute of Technology Zhang, Shengping ; Harbin Institute of Technology Feng, Jiang; Harbin Institute of Technology, Computer Science and Technology Liu, Jie; Harbin Institute of Technology Ding, Zhen; Harbin Institute of Technology Yang, Chifu; Harbin Institute of Technology Zhou, Huiyu; University of Leicester
Keywords:	Full kinetics, Exoskeletons, Trustworthy RAS, Inertial measurement unit, Motor intent

SCHOLARONE™
Manuscripts

Enable Fully Customized Assistance: A Novel IMU-based Motor Intent Decoding Scheme

Chunzhi Yi, Shengping Zhang, Feng Jiang*, Jie Liu, Zhen Ding, Chifu Yang, and Huiyu Zhou

Abstract—Trustworthy human-exoskeleton interaction essentially relates to determining the assistive force profile. Current methods of decoding human motor intent enable the customized determination of the assistive force profile by providing limited information of human kinetics. In this paper, we propose and validate a novel motor intent decoding scheme that can enable a fully customized assistive force profile, where only inertial measurement units (IMUs) are used. First, we improve the robustness of the IMU-based kinematic estimation by sampling IMU measurements that well meet the hinge-joint assumption, and by online calibrating axes' direction in order to avoid the post-hoc analysis of joint axes' directions during the determination of the body-fixed coordinate frame. Second, using the calculated kinematics as input, we develop a computationally efficient dynamic model, through which kinetics of users can be calculated in real-time. Finally, we leverage a cable-driven ankle exoskeleton method to validate the assistive performance of our motor intent decoding scheme. We perform experiments on ten healthy subjects to evaluate the accuracy of our algorithm, and the change of metabolic rate and muscle efforts under the exoskeleton's assistance. The results show the improvement from determining the assistive force profile by nominal curves and the feasibility of our algorithm.

Index Terms—Full kinetics, Exoskeletons, Trustworthy RAS, Inertial measurement unit, Motor intent.

I. INTRODUCTION

RECENT development of artificial intelligence and edge computing (AIEC) plays a significant role in improving the trustworthiness of robots and autonomous system (RAS) [1–3]. As indicated in [4], AIEC enables the trustworthy RAS to interact with humans through mixed human-robot initiative and interpretable human-robot interaction. In designing trustworthy human-exoskeleton interactions, AIEC-enabled motor intent decoding schemes provide reference signals of users' biological efforts for the customized assistive force profile, thus fundamentally relate to the mixed initiative of the human-exoskeleton system and interpretable

Chunzhi Yi and Zhen Ding are with the School of Mechatronics Engineering, Harbin Institute of Technology, Harbin, Heilongjiang, 150001 China.

Shengping Zhang is with the School of Computer Science and Technology, Harbin Institute of Technology, Weihai 264209, China.

Jie Liu is with the AI Research Institute, Harbin Institute of Technology, Shenzhen 518055, China.

Chunzhi Yi and Feng Jiang are with the School of Computer, Harbin Institute of Technology, Harbin, Heilongjiang, 150001 China and Pengcheng Laboratory, Shenzhen, Guangdong, China e-mail: fjjiang@hit.edu.cn(F.Jiang).

Huiyu Zhou is with the School of Informatics, University of Leicester, Leicester LE1 7RH, U.K.

improvements of human motor performance. Studies report that the customized assistive force profiles, enabled by various motor intent decoding schemes, are effective for reducing muscle effort or metabolic cost [5–7]. Furthermore, as reported in a comparison study [8], a more subject-specific assistance can enable a better assistive performance. People can naturally infer that an ideal motor intent decoding scheme for exoskeletons is supposed to be capable of providing full information of users' efforts to enable a fully customized assistive force profile.

Essentially, exoskeletons' assistance is derived from the assistive force profile. A motor intent decoding scheme could enable a customized assistive force profile from four aspects: timing, magnitude, shape and duration. To this end, it leverages signals highly related to lower-limb kinetics, such as the interactive force, kinematic and electromechanical signals of human. Among such signals, the most natural one is the interaction force signals from pressure insoles or other force sensors [9–11]. These force or pressure sensors, although can provide direct interaction information, can only determine the timing of assistance. In addition, they might lead to a cumbersome mechanical structure of robots or be prone to severe intent misjudgment caused by an unanticipated collision from environment [12]. Kinematic signals, reflecting insightful gait information, is now increasingly used in exoskeletons' control. In a kinematics-based motor intent decoding schemes, the assistive torques are activated at subject-specific timings by detecting key features of gait or gait phases. For example, Ding et al. proposed to use the zero-crossing point of angular velocity to detect the timing of assistive torque [13]. A study presented by Zhang et al. determined the assistive force profile according to a desired angle-to-moment curve [14]. Some other studies predicted discrete or continuous gait phases to provide reference force signals for assistance [15–17]. Such works, although indicate a subject-specific timing of the assistive force profile, are difficult to give the information of the remaining three aspects, thus could suffer from an inferior customization. Although human-in-the-loop optimization can be applied to tuning the remaining parameters [18, 19], as argued in [7], assistance parameters are often fixed after optimization, even when users may still be changing their patterns. Assistance based on decoding myoelectric signals (EMG), including pattern classification [20], continuous proportional control [21], and continuous non-linear control with or without neuromuscular models [16, 22], could reflect the activation

of relative muscles and thus determine a subject-specific assistive force profile. However, the nonlinear and time-varying characteristics of EMG impedes its customized application on exoskeletons, especially in need of providing a stable assistance with good generalization capabilities across different subjects.

To address these limitations, there is recent interest in developing a novel motor intent decoding scheme for exoskeletons that can provide full kinetic information thus enable a fully customized assistive force profile with stable signals, if possible, with simple sensors. To do so, the recent development of inertial measurement unit (IMU)-based kinematic and kinetic assessment methods is exploited and explored to build an inverse dynamic model of human with IMU measurements, based on exploring the lower-limb kinematic constraint, ground-foot wrench and the biomechanical principles of locomotion. This could lead to a potential application under multiple locomotion patterns and gait phases.

Specifically, a kinematic constraint is adopted to make the IMU-based kinematic estimation free of sensor alignment. An effective sampling of IMU signals is proposed to improve the robustness of the kinematic estimation. After transforming the IMU measurements into human segments' kinematics, a 7-link inverse dynamic model that aims at decreasing sensor amount and computational load is then developed to calculate kinetics with the estimated kinematics. During the double support phase, the ground-foot contact wrenches acting on both feet contribute to an indeterminate dynamical balance problem. As a result, the lower-limb kinetics cannot be calculated by the inverse dynamic model. The "smooth transition assumption (STA)" is adopted to infer ground-foot contact wrenches during double support phase, which solves the indeterminacy problem.

The main contributions of our paper can be summarized as follow:

- We propose a novel motor intent decoding scheme for lower-limb exoskeletons that can fully determine customized assistive force profiles based on an inverse dynamic model solely using IMU measurements.
- Due to the cascade calculation of kinematics and kinetics, we further improve the algorithm's accuracy through effective sampling of IMU signals and the online calibration of axes' direction.
- By comparing the assistive performance of joint moment calculated by our algorithm and a nominal joint moment, we demonstrate the feasibility of our algorithm and the benefit of determining fully customized assistance.

This paper is organized as follows: In section II, the challenges and employed methods of our algorithm are introduced. Section III describes the methodology and implementation of our algorithm. The experimental validation is presented in Section IV. The discussion and conclusion are shown in Sections V and VI.

II. RELATED WORK

With the aim of calculating lower-limb moment with IMU measurements, we need to address some issues. Firstly, the algorithm of estimating kinematics, as the base of the whole algorithm, is of vital importance. Such an algorithm should avoid the usage of careful sensor-to-body alignment or calibration procedure and presents enough robustness against sensor noise. Secondly, we employ an inverse dynamic model by carefully balancing accuracy and computational efficiency. Thirdly, by excluding foot pressure sensors, a practical ground-foot contact model should be adopted to estimate ground reaction wrenches of each foot during the double support phase. The parameters and implementation of the model should be online achievable. The remaining of this section details the three challenges.

A. Robust Algorithm For Estimating Lower-Limb Joint Kinematics

Traditionally IMU-based estimation of lower-limb joint angles employed various calibration postures and/or careful IMU-to-body alignment [23–27] which limited its real-time application on controlling exoskeletons. Recently, Seel et.al. precluded the usage of calibration postures or sensor alignment by applying an gyroscope-related biomechanical constraint to estimate joint axes and joint position vectors [28]. However, the angular rate-related constraint, which was employed in estimating joint axes, has been demonstrated in [29] to be inaccurate under some certain circumstances. Inspired by [29], we employ the weighted summation of gyroscope-based and accelerometer-based constraints as cost function to estimate joint axes. Another problem that might cause accuracy deterioration remains in the hinge-joint approximation of above mentioned biomechanical constraints. Although the characteristics of lower-limb joints during locomotion rationalizes approximating these joints as a hinge joint, the 3-DoF biological structure of lower-limb joints sometimes might invalidate the approximation. To this end, we propose to sample effective points from IMU measurements, which meet the hinge-joint approximation, and iteratively estimate joint axes to improve the robustness and the accuracy of the estimation.

In addition, the joint axes estimated by the biomechanical constraint are bidirectional, the directions of which need to be determined. In Seel's work [28], the axes' directions were calibrated post hoc by the orientation of the mounted sensors relative to the desired joint axes or the traces of the angular rates projected in local joint planes. Both of them require post-hoc analysis. In this article, an online calibration of joint axes' directions is performed in real time by utilizing the cyclic characteristics of gait.

B. The Inverse Dynamic Model of Human

When considering the inverse dynamic model's accuracy and computational efficiency, the segments that denote the upper limbs should be carefully modelled. Previous studies

[30, 31] modelled upper limbs as three segments in order to create a 3-dimensional (3D) dynamic model. In our algorithm, we only sought to calculate lower-body joint moment in the direction of flexion/extension, i.e. to develop a 2-dimensional (2D) dynamic model on the sagittal plane. Thus, we simplify the upper limbs as one single link in order to improve the computational efficiency.

In addition, the mechanics method in the modelling results in different performances. If the Lagrange method is used, the inverse dynamic model can be developed in an analytical manner. But the switches of multiple ground-foot contact conditions will cause discontinuousness, which will lead to the model's sensitivity to modelling errors [32]. In order to avoid this potential bottleneck, we employ the Newton-Euler method to develop our inverse dynamic model.

C. Practical Ground-Foot Contact Model For Real-Time Application

Predicting indeterminate ground-foot contact wrenches, i.e. the ground reaction forces (GRFs) and the ground reaction moment (GRM), during the double support phase is pivotal for the inverse dynamic model. Most currently used methods developed for biomechanical analysis and bipedal robot are impractical for our algorithm. To be specific, machine learning-based methods, such as [33] and [34], predict the 3D ground-foot contact wrenches accurately. However, the generalization of such methods conflicts with the need of real-time parameter identification, which impedes the real-time application in our algorithm. Model-based methods treat the ground-foot contact wrenches as the function of the indentation between spheres and the ground [35, 36], and then optimize the function. The excessive variables for optimization reduce the computational efficiency and make the methods unsuitable for online parameter identification and its consequent usage in our algorithm. Other methods that were applied on a bipedal robot and robotic exoskeletons is also unsuitable due to the lack of accurate estimation of inertia, damping and stiffness terms of human segments.

Compared with the abovementioned methods, the "smooth transition assumption (STA)" benefits from its lesser parameters and validity for mimicking ground-foot contact wrenches of the support foot during the double support phase on the sagittal plane [37]. In this article, STA is employed to predict each 2D ground-foot contact wrench.

III. ALGORITHM DEVELOPMENT

The whole working flow of our algorithm is presented in Fig. 1. We firstly use the IMU signals to calculate the coordinates of the joint axes and the sensor position vectors. Then, the body-fixed coordinate frames are determined by the estimated joint axes and the accelerometer measurements during an initial stand. In virtue of the body-fixed coordinate frames and the pseudo-periodic characteristics of lower-limb kinematics, we propose an online method of determining the directions of joint axes. Thirdly, we estimate the kinematics of each segment. Finally, the estimated kinematics is fed

into a 2D inverse dynamic model to calculate kinetics of the lower limbs.

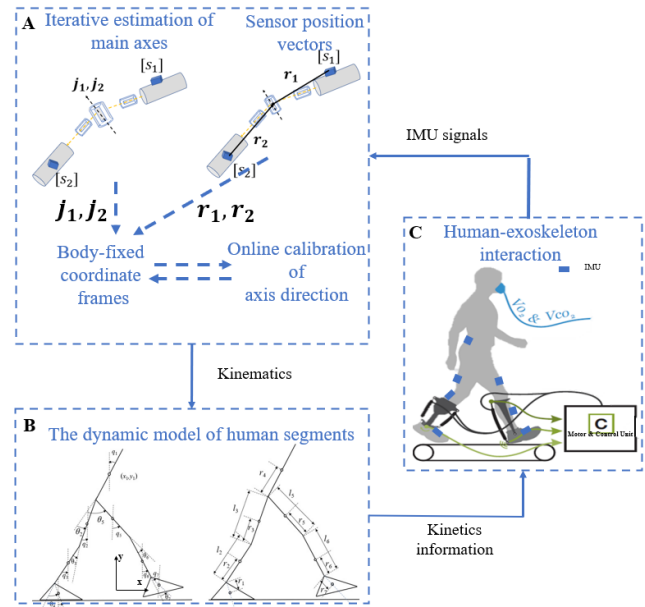


Fig. 1. The working flow of the motor intent decoding scheme. Firstly, IMU signals measured from human subjects are used to estimate joint axes and joint position vectors, and then to build body-fixed coordinate frames with the help of online calibration of the axes' directions. Secondly, IMU measurements are transformed to kinematics through the body-fixed coordinate frames, and then fed into dynamic model of human segments. Finally, the calculated kinetics is leveraged to determine the assistive force profile and to apply on human subjects, where j_1, j_2 denote main axes, r_1 and r_2 denote joint position vectors.

A. Kinematic Estimation

Due to the cascade calculation of kinematics and kinetics, we render high importance on the robustness and accuracy of the kinematic estimation. To this end, based on the adopted 1-DoF biomechanical constraint that estimates main axes of lower-limb joints through a hinge-joint approximation, we further propose a method of sampling effective IMU signals to select IMU measurements that meet the approximation. In this way, the joint axis estimation and the effective point sampling can be applied iteratively to achieve a more robust estimation. Furthermore, the body-fixed coordinate frames are determined by the estimated axes and the sensor position vectors using the method of [28], where the principle of lower-limb movements is leveraged to determine the joint axes' directions without post-hoc analysis. Finally, we estimate kinematics within the body-fixed coordinate frames.

1) *Joint Axis Estimation with IMU Measurement Sampling*: The work flow of iteratively estimating the main axes of each lower-limb joint is shown in Fig. 2.

The 1-DOF Biomechanical Constraint: The existence of joint axes, around which lower-limb joints rotate in the most time during a gait cycle, rationalizes simplifying such joints as hinge joints [28, 29]. Such axes usually correspond to the rotation of each lower-limb joint on the sagittal plane.

Adopted in [29], the biomechanical constraint of lower-limb joints, which is based on the hinge-joint approximation,

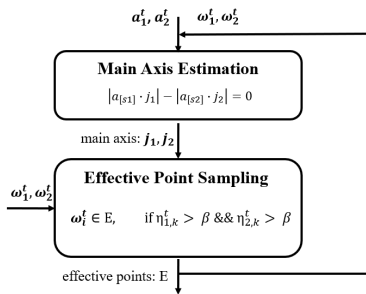


Fig. 2. The working flow of estimating joint axes. The 1-DoF biomechanical constraint are employed to initialize the coordinates of the joint axes, which are then used to sample the effective points. The iterative loop is set to be performed three times.

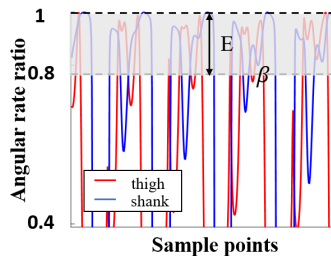


Fig. 3. The angular rate characteristics of the lower-limb joints.

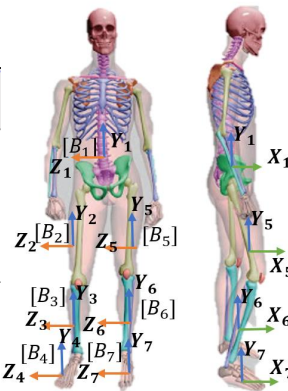


Fig. 4. The orientation relation of IMU mounted to the trunk.

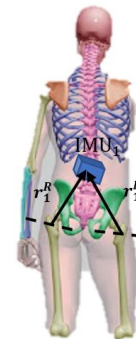


Fig. 5. The orientation relation of the IMU mounted to trunk, where r_1^R and r_1^L denote the sensor position vectors of right and left hips relative to the IMU mounted on the upper limb.

is the weighted summation of gyroscope-based (H_g) and accelerometer-based constraints (H_a). The weight of H_a is set to be 0.6. We construct the biomechanical constraint as cost function and employ the least-square method to solve this non-linear minimizing problem. As shown in Fig.1 A, j_1 and j_2 denote the joint axis of a lower-limb joint described in different sensor-fixed coordinate frames $[s_1]$ and $[s_2]$, respectively.

Sampling IMU Measurements For The Biomechanical Constraint: The joint axis estimated by the 1-DOF constraint above suffers from theoretical errors, which result from the deviation between the hinge-joint approximation and the 3-DOF biological structure of lower-limb joints. Due to the deviation, the angular rates of segments cannot always coincide with the estimated axis. To make quantitative metrics, we calculate the angular rate ratio η_i^t , which denotes to what degree the rotation of the biological joint meets the hinge-joint assumption.

$$\eta_i^t = \frac{|\omega_i^t \cdot j_i|}{\|\omega_i^t\|} \quad (1)$$

where η_i^t denotes the instant angular rate ratio of each segment, ω_i^t denotes the measured angular rate of each segment, i demotes segment and t denotes time instant. Fig. 3 illustrates the angular rate ratio of each segment. It can be seen that there are some periods of a gait cycle during which the angular rate ratio is approximately equal to one. During those periods, the lower-limb joints function approximately as a hinge joint. The sampled measurements during such instances are named as effective points while the other sampled measurements are named as interferential points. Obviously, involving such interferential points into the joint axis estimation would contribute to a deviation toward other rotational axes of the 3-DOF lower-limb joint.

Herein, we set a threshold to distinguish the effective points and the interferential points based on the comparison

with the angular rate ratio, which is given by

$$\omega_i^t \in E, \text{ if } \eta_1^t > \beta \& \eta_2^t > \beta, \quad (2)$$

where $\beta \in (0, 1)$ denotes the threshold for the effective point sampling, which is set to be 0.85.

The Lower-Limb Joint Axis Iterative Estimation: As shown in Fig. 2, to further improve the estimation accuracy, we combine the sampling of effective points and the joint axis estimation in an iterative manner. For all the sampled measurements as effective points, the initial joint axis is estimated using the 1-DOF biomechanical constraint. Substituting the estimated axis into Equation (1), we calculate the angular rate ratio for each segment-to-joint couple in order to determine the effectiveness of the sampled measurement through a comparison with the threshold. It can be seen from Fig. 2 that the input of the joint axis estimation is replaced by E , the set of effective points, in order to gradually reduce the error caused by the 3-DOF rotation of lower-limb joints around other two axes. The updating of the set E contributes to a convergent estimation of the axis. The iteration times are set to be 3.

2) *The Determination of The Body-Fixed Coordinate Frames:* The body-fixed coordinate frames are determined to provide a reference for calculating kinematics.

Firstly, we estimate the sensor position vectors, which work as a component, by the method of [28]. The sensor position vectors r_1^k and r_2^k , $k = R, L$ that denote the vectors from the origin of the sensor-fixed coordinate frame to the rotation center of the biological joint, can be estimated based on the 3D constraint of accelerations. R and L denote right and left leg, respectively.

Secondly, we construct the body-fixed frames as shown in Fig. 4. Different from the joint coordinate system recommended by ISB, the body-fixed frames are defined with perpendicular coordinate axes where z_i -axis coincides with the estimated joint axis, x_i -axis is the cross product of the main axis and the sensor position vectors, and y_i axis is vertical to the $x_i z_i$ plane.

Herein, we construct the direction cosine matrix between the sensor-fixed and body-fixed coordinate frames as

$$R_{b_i}^{s_i} = [x_i, y_i, z_i] \quad (3)$$

where x_i , y_i and z_i denote the coordinate axes of the body-fixed coordinate frames determined above.

3) *Online Calibration of Axes' Directions:* During the joint axis estimation, the direction of the vector j_i cannot be determined by the optimization process, which might contribute to difference directions of the estimated axes of each joint. If so, the joint axis-constructed body-fixed coordinate frames might have different directions. In [28], Seel et al. corrected the direction of the main axis according to the given sensor placements or the traces of the angular rates projected onto local joint planes. Both methods need a post-hoc analysis. Therefore, in order to avoid the manually tuning process, it is necessary to develop an online method of calibrating the direction of the vector j_i .

Axis Direction Calibration For IMUs on The Thigh, Shank and Foot: According to proportion 1 in the Appendix, during a gait cycle, there are always elements in A_{thigh} that are the opposites of those in B_{thigh} , while the contrary condition occurs in pairs, such as (A_{shank}, B_{shank}) and (A_{foot}, B_{foot}) . Thus, we can calibrate the direction of the estimated joint axis online by discretely summing such projections over cycles.

$$\begin{aligned} \hat{j}_i &= j_i, \text{ if } \sum a_t \cdot x_t > 0 \text{ OR } \sum a_{a/f} \cdot x_{a/f} < 0 \\ \hat{j}_i &= -j_i, \text{ if } \sum a_t \cdot x_t < 0 \text{ OR } \sum a_{a/f} \cdot x_{a/f} > 0 \end{aligned} \quad (4)$$

where \hat{j}_i denotes the main axis, x denotes the x axis of the body-fixed coordinate frame, a denotes measured accelerations, the subscripts t , a and f denote thigh, shank and foot, respectively.

Axis Direction Calibration for IMU on The Trunk: Due to the small magnitude of the trunk dip angle, we can hardly calibrate the direction of the joint axis depicted in the sensor-fixed coordinate frame on the trunk by applying proposition 1. Another strategy needs to be performed in this scenario. As shown in Fig. 5, the measurements of the IMU on the trunk is used to estimate the joint position vectors of bilateral hip joints. The cross product \tilde{x}_1 of the two joint position vectors, r_1^R , r_1^L , has the direction similar to the x_1 axis of the body-fixed frame of the trunk.

$$\begin{aligned} \hat{j}_i &= j_i, \text{ if } j_i \cdot d > 0 \\ \hat{j}_i &= -j_i, \text{ if } j_i \cdot d < 0 \end{aligned} \quad (5)$$

where $\tilde{x}_1 = r_1^R \times r_1^L$, $d = \tilde{x}_1 \times y_1$

4) *Calculating Kinematics:* On this basis, we can estimate the kinematic data in the body-fixed coordinate frames, which will feed into the 2D inverse dynamic model.

Angles: We estimate the lower-limb joint angles by the data fusion method. Details are shown in [28]. When walking, the range of the dip angle of human upper limbs is (-2 deg, 2 deg). Herein, the dip angle is set to be zero.

Angular Rates: We calculate the angular rate of a lower limb joint by the difference between the projections of the measured angular rates on the main axes.

Angular Accelerations: We calculate the angular acceleration of the lower limb joint as the finite difference of angular rates.

Linear Accelerations: Note that only the linear acceleration of the upper limb needs to be calculated because the inverse dynamic model is formed based on the center of mass of the upper limb. Considering the dip angle of upper limb is set to be zero, the linear acceleration of upper limb's CoM which is described in the global coordinate frame (Fig.6), can be estimated as follows

$$\tilde{a}_{upper}^{b_1} = \begin{bmatrix} 1 & 0 & 0 \\ 0 & 1 & 0 \end{bmatrix} \cdot (R_{b_1}^{s_1} \cdot a_{upper}^{s_1}) \quad (6)$$

where $\tilde{a}_{upper}^{b_1}$ denotes the 2-element linear acceleration of the upper limb described in the global coordinate frame in Fig. 6, $a_{upper}^{s_1}$ denotes the linear acceleration of the upper limb described in the sensor-fixed coordinate frame $[s_1]$, which is the measurement of the accelerometer.

B. Kinetic Calculation

The calculated kinematics is fed into a 2D, 7-link inverse dynamic model. We employ the model to approximate the dynamics on the sagittal plane and to calculate the joint moment of the lower-limb joints. In this section, we firstly develop the inverse dynamic model, and then calculate the kinematics and dynamics based on this model.

1) *A Simplified Human Body Model:* In Fig. 6, we regard the whole upper body as one segment and simplify the inverse dynamic model of the human body as a 9-DoF, 7-link multibody system. The links denote the upper body, thigh, shank and foot respectively and can rotate around their linked joints. The multibody system translates based on the movements of the upper limbs' center of mass. We leverage the equations used in [38] to estimate each segment's inertia and geometric parameters from the anthropometric measurements of each subject's height and weight. Compared with the models proposed in [30] and [31], our model significantly simplifies the upper-limb part and keeps the each lower-limb segment in order to maintain the accuracy.

2) *Kinematic Expression:* In the following, we formulate the kinematic law of the 2D model to calculate each segment's accelerations. Treating the upper limb's CoM as the float base of the model, we describe the positions of each segment's CoM by joint angles, the upper limb's CoM and each segment's geometric parameters. The detailed formulations follow the work of [39].

It should be noted that we can define the global coordinate frame's origin as any point on the ground since we only care about the relative positions of the segments.

Taking the kinematic expression's second derivative against time, we can obtain the relationship between the acceleration of each lower-limb segment's CoM and that of the upper limb's CoM. We then plug the linear and angular

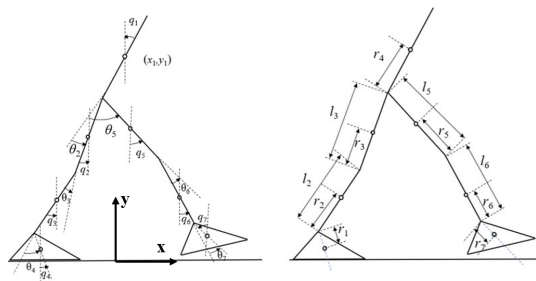


Fig. 6. The simplified human body model. Where q_i denotes the i th segment's dip angle, θ_i denotes the i th joint's angle, (x_i, y_i) denotes the coordinates of the i th segment's CoM in the global coordinate system, l_i denotes the i th segment's length, r_i denotes the distance of the i th segment's and the joint's CoM.

accelerations of joints and segments estimated by III-A4 into the relationship. In so doing, we can calculate the horizontal and vertical accelerations of each segment's CoM and then feed them to the inverse dynamic model.

3) *Dynamical Expression*: Here, we develop the inverse dynamics of the multibody model with the empirical model of the ground-foot contact wrenches. Herein, we develop dynamical expressions using the Newton-Euler method, in order to reduce the sensitivity of the modelling errors. The detailed expressions are similar to those shown in [30], the difference is that we only calculate kinetics on the sagittal plane.

During the single support phase, we can directly estimate the GRF and GRM of the support foot. Because the GRF and GRM of the swing leg are zero, the ground-foot contact wrenches of each leg are determined. That is, we can solve all the force and moment balance equations of the inverse dynamic model in order to derive all the internal forces and moment of each joint.

As for the double support phase, we can calculate GRFs' and GRMs' summations of both legs with the same procedure. Due to the indeterminate dynamics of the double support phase, we cannot directly calculate the GRF and GRM of either leg. To solve this problem, we employ the "smooth transition assumption (STA)" proposed by [32] to estimate the GRM's and GRF's ratio of the supporting leg. Using these ratios, we can calculate the GRFs and GRMs of each leg so that the indeterminate dynamic problem is solved.

IV. EXPERIMENT

In order to validate the proposed algorithm and its performance on exoskeleton, the experiments are threefold. First, we validate the accuracy of the kinematic estimation algorithm, while we also demonstrate the algorithm's robustness against measurement noise. During the sensitivity test, a comparison is made against Seel's work to validate the feasibility of our proposed IMU measurement sampling. Second, we validate the accuracy of joint moment estimation against the data measured by the ground reaction force plates and the optimal motion capture system. Finally, we test the

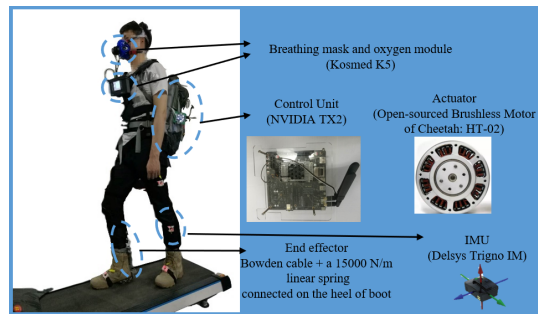


Fig. 7. The lateral view of a person wearing the experimental setup. The following components are visible: breathing mask and oxygen module, a bag with control unit and actuator, the sensory system of IMUs, and the boot instrumented with end effector.

assistive performance by applying our algorithm on an ankle exoskeleton.

The experiment protocol is approved by the local ethical committee and all the participants have been informed of the content and their right to withdraw from the study at any time, without giving explanation.

A. Experimental Set-Up

1) *Kinematic and Kinetic Estimation*: The algorithm is tested on ten healthy subjects (age: 25 ± 3 year, weight: 69.5 ± 8 kg, height: 1.72 ± 0.15 m) walking on the level ground. All the subjects have signed the written consent for participating in this experiment. 7 IMUs (Delsys Trigno IM, sampling frequency: 148 Hz) is rigidly mounted, six on lower-limb segments and one on the lower back. It should be noted that the IMU on the lower back should be mounted visually close to the CoM.

In order to verify the algorithm, we employ the Vicon optical tracking system (Vicon Motion Systems, Ltd.) and force plates to measure the kinematic data, the GRFs and the GRMs. Both the optical tracking system and the force plates sample signals at the frequency of 100 Hz. All the measurements are triggered by the synchronizer and then synchronized by time stamps.

2) *Experiments on The Exoskeleton*: The assistance is provided by a cable-driven ankle exoskeleton worn by subjects. A person wearing the full experimental setup is shown in Fig. 7. Other than IMUs, we also place EMG sensors (Delsys Trigno IM, sampling frequency: 1111 Hz) on soleus. The breathing mask and oxygen module (Cosmed K5) are used to measure the metabolic cost of subjects. We employ our algorithm as the motor intent decoding method of the exoskeleton to predict subject-specific joint moment, while we employ the PID control strategy as the low-level control to transmit the desired assistance into motor demands (the RMSE of tracking an ankle moment curve was 3.54 Nm on average). The magnitude of the assistive torque is 20% of the estimated ankle moment.

During all the experiments, an embedded control unit (NVIDIA TX2) is used to take the IMU data and perform

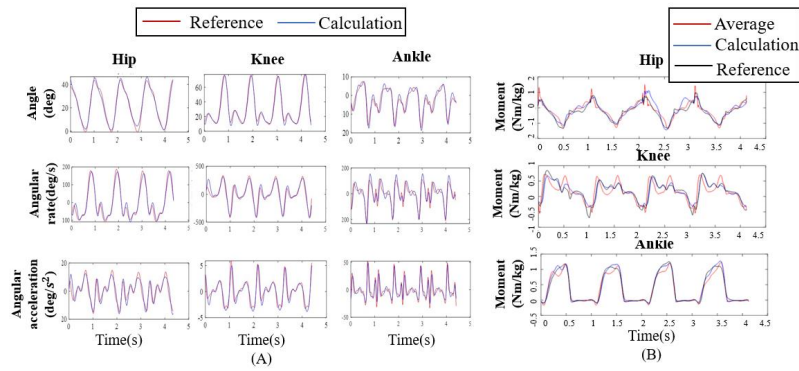


Fig. 8. Representative plots. (A) Calculated kinematics on the sagittal plane. Red lines (“Reference”) denote the reference curves by the optical motion capture systems; Blue lines (“Calculation”) denote the curves calculated by the algorithm. (B) Calculated kinetics on the sagittal plane. Red lines (“Average”) denote the curves averaged over the calculated joint moment of the ten subjects; blue lines (“Calculation”) denote the curves of the calculated joint moment of one subject; Black lines (“Reference”) denote the reference curves of the same subject.

kinematic and kinetic estimations. The Python-based program in the embedded control unit has three functions: 1) communicate with the Delsys software on a PC to collect signals from the seven IMUs; 2) store the IMU and EMG signals, the estimated joint moments and angles for the off-line analysis; 3) generate a control signal based on the inverse dynamic model and control the motor to provide mechanical torque through the ankle exoskeleton.

B. Experiment Protocol

1) *Kinematic and Kinetic Estimation*: During this test, the subjects are asked to perform three trials of walking on the ground reaction force plates with reflective points and IMUs. Each trial consists of a 10s standstill, a 2-min walking with self-selected speeds on the ground reaction force plates and a 1-min rest. The IMU data and the calculated joint moment and kinematics are stored in the embedded control unit.

2) *Assistance From The Exoskeleton*: Before starting the experiment, each subject undergoes a phase of 10-min animation, during which the subject walks on a treadmill with exoskeleton at a constant speed of 4.5km/h. Due to the unidirectional actuation, the exoskeleton only assists plantar flexion. Afterward, all the subjects undergo a series of 20-min walking tests and 5-min rest for three times under the following conditions:

- Passive Exo (pas)—ground-level walking on the treadmill wearing the ankle exoskeleton but without assistance.
- Active Exo1 (act1)—ground-level walking on the treadmill with customized assistance.
- Active Exo2 (act2)—ground-level walking on the treadmill with assistance from the ankle exoskeleton. The assistance is provided according to the nominal curve of ankle moment [40] as reported in [6, 13].

TABLE I
THE ACCURACY OF THE KINEMATIC CALCULATION

Joint	Hip	Knee	Ankle
θ (deg)	2.41 \pm 0.51	2.61 \pm 0.67	2.14 \pm 0.33
$\dot{\theta}$ (deg/s)	19.54 \pm 5.63	27.63 \pm 4.37	25.66 \pm 7.81
$\ddot{\theta}$ (deg ² /s)	134.39 \pm 67.86	288.61 \pm 71.6	313.59 \pm 86.1
θ (deg) [28]	/	3.30 \pm 1.20	1.62 \pm 0.57

TABLE II
THE ACCURACY OF THE MOMENT CALCULATION

Joint	Hip	Knee	Ankle
RMSE(Nm/kg)	0.18 \pm 0.05	0.15 \pm 0.03	0.11 \pm 0.02
RMSE(%)	7.7% \pm 1.1%	13.1% \pm 2.3%	6.8% \pm 1.1%

^aThe percentages denote the ratio of RMSE and the amplitudes of joint moment.

C. Data Processing

The raw data is processed by MATLAB 2019. The kinematic data are filtered using a low pass zero lag fourth-order Butterworth digital filter with a cutoff frequency of 4.5 Hz.

We calculate RMSEs in order to validate the accuracy of each estimate. For quantifying the performance on the ankle exoskeleton, we assess the following items.

- The kinematics during walking, i.e. the hip, knee and ankle angles (from IMUs);
- The kinetics during walking, i.e. the joint moment of each lower-limb joint calculated by our algorithm, the joint moment of the nominal curves and the reference joint moment from the motion capture system.
- Metabolic cost of the subjects at different assistive conditions.

V. RESULTS AND DISCUSSION

A. The Accuracy of Kinematic Estimation

Results of joint angles are presented in Fig. 8 (A). Four intact gaits are depicted with angles, angular rates and angular accelerations of each lower-limb joint. It can be seen that the estimated curves are close to the references. Table I presents the accuracy of the estimates. The accuracy is depicted in the way of mean \pm SD. The percentages in brackets denote the proportion of the means to the magnitudes. It is shown that the mean square deviation of the knee angle is 2.61 deg. The mean square deviation of the ankle angle is 2.41deg. The mean square deviation of the hip angle is 2.14 deg. This performance presents a comparable accuracy against those of [28].

B. Robustness Improvement Through Effective Point Sampling

For each subject, 10 pieces of data are arbitrarily taken as input data. The selection process is completely random.

Using each piece of data, 10 direction vectors of joint axes can be solved. In order to measure the stability of algorithms, the radius of the minimum envelope cone of the 10 axes is calculated as metrics, as shown in Fig. 9. In this section, we compare our algorithm with the work [28], and the cone radius of which are denoted by R_a , R_w . R_a is 0.16 ± 0.08 , while R_w is 0.23 ± 0.08 . The axes estimated by our algorithm have less divergence compared with those estimated from the Seel's algorithm. This result demonstrates that our method of estimating joint axes is of more robustness.

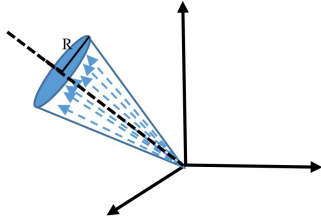


Fig. 9. The schematic diagram of how to quantify the robustness

As mentioned previously, when estimating the joint axis, sampling the IMU measurements iteratively improves the stability of the algorithm. Seel et al. established a constraint equation based on the hinge joint approximation without considering whether the input data met this approximation [28, 29], thus ignored the importance of sampling effective points from input data. Thus, we propose the effective point sampling method based on the angular rate ratio, which further increases the robustness based on the deeper exploration of biomechanics. By comparing the robustness of the two methods, we can demonstrate that iteratively sampling IMU measurements can improve the stability of estimating the joint axes.

C. Accuracy of The Kinetic Calculation

As shown in Fig.8 (B) and Table II, the mean square deviations of joint moment are: 0.18 ± 0.05 Nm/ kg (7.7%) for hip, 0.15 ± 0.03 Nm/ kg (13.1%) for knee and 0.11 ± 0.02 Nm/ kg (6.8%) for ankle. We evaluate the accuracy by comparing the calculated moment and the reference moment. In Fig.8 (B), we present the representative plots of one subject, the averaged moment curves calculated from ten subjects and the reference moment curves. The calculated moment is similar to the reference curves. As shown in Table II, the RMSE of each joint increases from the distal joint to the proximal joint.

The increasing trend of RMSEs gives insightful information of our inverse dynamic model's accumulated modeling error. The joint moment's calculation starts from the distal joint to the proximal joint. Due to the simplified model, the inverse dynamic modeling errors, the kinematic estimation errors and the errors of ground-foot contact model parameters accumulate when calculating the distal joints' or segments' force and moment. This trend meets the results reported in [30]. In addition, the performance of

our algorithm outperforms the SOTA performance presented in the literature. In [30], the moment errors depicted by the percentage of each joint moment's magnitude are 9.7% for ankle, 18.7% for knee and 20.9% for hip. The accuracies of [31] and [41] are 17.1% and 22.3% for knee. The accuracy of [42] is 7.2% for hip. Thus, we can conclude that our algorithm meets the accuracy demand of calculating the joint moment in the sagittal plane and providing reference signals for controlling exoskeletons.

D. Assistive Performance on The Exoskeleton

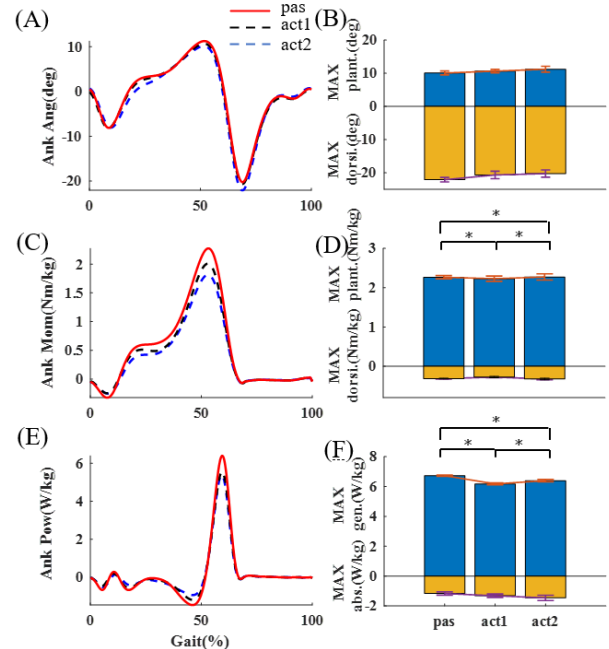


Fig. 10. Changes in ankle angles, moment and power. (A), (C), (E) are averaged angle, moment and power curves of ankle under different assistive modes; (B), (D), (F) are averaged biological maximum angle, moment and power on both directions where * denotes the statistically significant differences with the unpowered condition (ANOVA, $p < 0.050$). Pas, act1 and act2 denote the different assistive modes, related to passive exo, active Exo1 and active Exo2, respectively. Plant. denotes plantar flexion, dorsi. denotes dorsiflexion. Gen. denotes the power generated by ankle, abs. denotes the absorbed power.

As shown in Fig. 10, compared with the pas mode, the biological ankle moment and power of both active modes (act1 and act2) present significant difference, while no significant difference exists in kinematics. Specifically, the maximum biological ankle moment of act1 and act2 during plantar flexion are 2.23 ± 0.07 , 2.26 ± 0.08 Nm/kg, both of which are significantly smaller than that of pas (2.26 ± 0.04 Nm/kg). The maximum biological ankle power of act1 and act2 during plantar flexion of act1 and act2 are 6.18 ± 0.07 , 6.40 ± 0.08 W/kg, both of which are significantly smaller than that of pas (6.73 ± 0.04 W/kg).

As shown in Fig.11, we calculate the net metabolic rates by subtracting the metabolic cost of the pas mode from that of act1 and act2 modes. In addition, we evaluate the muscle effort by estimating the normalized root mean square (RMS)

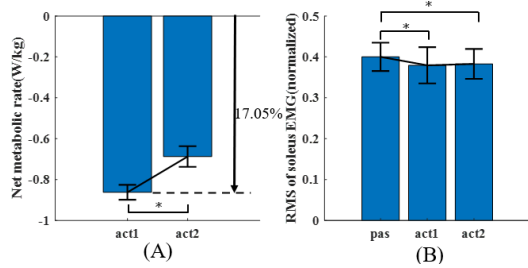


Fig. 11. Changes in metabolic rate and soleus activation. (A) presents net metabolic rate changes of act1 and act2 modes, compared with pas mode. Significant difference was found between the two modes (ANOVA, $p < 0.050$). The maximum metabolic rate reduction is 17.05%. (B) presents the RMS of soleus EMG during pas, act1 and act2 modes. Statistical differences are found (ANOVA, $p < 0.050$).

of soleus on the exoskeleton side. Compared with the pas mode, the act1 mode significantly reduces more metabolic cost and the effort of soleus. We can conclude that the assistive force profile determined by our algorithm is more energy efficient.

In this experiment, we compare the performance of the assistance determined by the real-time calculated joint moment curve (act1) and the nominal joint moment curve (act2) with the pas mode, where the assisted joint angle, moment and power are measured. It can be seen that there is no significant kinematic difference caused by the assistance, while the biological moment and power are reduced. The more reduction of act1 mode demonstrates that the full kinetic information-determined assistance performs better in replacing the biological function of the assisted joint without causing statistical difference of kinematics. In addition, we also demonstrate the full kinetic information-determined assistance (act1) outperforms in saving biological energy and muscle efforts, as indicated by the evaluation on the metabolic cost and the soleus' efforts. Therefore, we can conclude that the fully customized assistive force profile, enabled by our motor intent decoding scheme, can provide a more effective assistance. Moreover, the experiments also reveal that the better assistive performance the exoskeleton can be achieved by providing more subject-specific information.

E. Limitations

The presented study has some limitations. First, the joint moment estimation algorithm is evaluated using an ankle exoskeleton. Simultaneously assisting all the lower-limb joints would further demonstrate the effectiveness of the algorithm. Second, the model for estimating the ground-foot contact wrenches is limited to the level walking condition. Alternative models should be employed to use our algorithm under other locomotion conditions.

VI. CONCLUSION

In this study, we have developed a motor intent decoding scheme solely using IMUs that can provide full kinetic information to determining the fully customized assistive force

profile for lower-limb exoskeletons. In our algorithm, we propose the effective point sampling of IMU measurements and the online calibration of axes' directions to integrate with the usage of current IMU-based kinematic estimation works, in order to improve the robustness and accuracy of kinematic estimation significantly. Moreover, based on the test on the ankle exoskeleton, we comprehensively evaluate the benefit of fully customized assistance with multiple metrics (e.g. kinematics, kinetics, energy and muscle efforts). This result reveals the benefits of determining assistance with more subject-specific kinetics information. The promising result will aid the control strategy design of lower-limb exoskeletons. Future work will include evaluating our algorithm with hip and knee exoskeletons, employing ground-foot contact models of other walking conditions and analyzing user experience with questionnaire-based evaluations.

APPENDIX A PROPOSITION 1

Dip angle of a lower-limb segment is denoted by the acute angle between y_i axis and the gravitational acceleration. In order to determine and correct the axis direction, a proposition should be firstly proposed and roughly proved according to the periodic characteristics of dip angles.

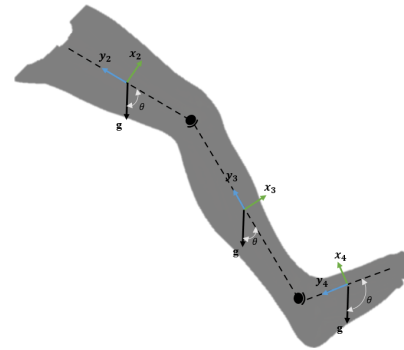


Fig. 12. Schematic diagram of the relation between y_i axis of body-fixed coordinate frames and the gravitational field vector.

Proposition 1: For any given periodic motion with relatively small movement-caused accelerations, the projection of a segment's acceleration on the x_i axis of its relative body-fixed frame is integrated over periods to be either positive or negative.

Proof. Let T denote the cycle length of a periodic lower-limb motion, A denote the set of positive dip angles of a segment (i.e. thigh, shank or foot) during one cycle and B denote the set of non-positive dip angles during the same cycle. According to the definition of dip angle, the integration of the acceleration projection over T is given by:

$$\begin{aligned} \int_0^T \mathbf{a}^t \cdot \mathbf{x}_i dt &= \int_0^T (\mathbf{a}_{move}^t + \mathbf{g}) \cdot \mathbf{x}_i dt \\ &\simeq \int_0^T \mathbf{g} \cdot \mathbf{x}_i dt \end{aligned}$$

$$\begin{aligned}
&= \int_0^T \|\mathbf{g}\| \|\mathbf{x}_i\| \cos(\theta + \frac{\pi}{2}) dt \\
&= -\|\mathbf{g}\| \left(\int_A \sin(\theta) dt + \int_B \sin(\theta) dt \right) \quad (7)
\end{aligned}$$

where a_{move}^t is the time-variant acceleration caused by segment movements, which can be neglected due to the small-movement assumption. Thus, we can approximately conclude that the integration is either positive or negative over motion cycles, given that the integration over A and B can hardly be equal in number. \square

REFERENCES

- [1] U. D. Ani, H. He, and A. Tiwari, "Human factor security: evaluating the cybersecurity capacity of the industrial workforce," *Journal of Systems and Information Technology*, 2019.
- [2] M. Desai, K. Stubbs, A. Steinfeld, and H. Yanco, "Creating trustworthy robots: Lessons and inspirations from automated systems," in *Proceedings of the AISB Convention: New Frontiers in Human-Robot Interaction*, April 2009.
- [3] T. Rezvani, K. Driggs-Campbell, D. Sadigh, S. S. Sastry, S. A. Seshia, and R. Bajcsy, "Towards trustworthy automation: User interfaces that convey internal and external awareness," in *2016 IEEE 19th International Conference on Intelligent Transportation Systems (ITSC)*, 2016, pp. 682–688.
- [4] H. He, J. Gray, A. Cangelosi, Q. Meng, T. M. McGinnity, and J. Mehnen, "The challenges and opportunities of artificial intelligence for trustworthy robots and autonomous systems," in *2020 3rd International Conference on Intelligent Robotic and Control Engineering (IRCE)*, 2020, pp. 68–74.
- [5] B. Quinlivan, S. Lee, P. Malcolm, D. Rossi, M. Grimmer, C. Siviyy, N. Karavas, D. Wagner, A. Asbeck, I. Galiana *et al.*, "Assistance magnitude versus metabolic cost reductions for a tethered multiarticular soft exosuit," *Sci. Robot*, vol. 2, no. 2, pp. 1–10, 2017.
- [6] L. M. Mooney, E. J. Rouse, and H. M. Herr, "Autonomous exoskeleton reduces metabolic cost of human walking during load carriage," *Journal of neuroengineering and rehabilitation*, vol. 11, no. 1, p. 80, 2014.
- [7] R. W. Jackson and S. H. Collins, "Heuristic-based ankle exoskeleton control for co-adaptive assistance of human locomotion," *IEEE Transactions on Neural Systems and Rehabilitation Engineering*, vol. 27, no. 10, pp. 2059–2069, 2019.
- [8] D. Ao, R. Song, and J. Gao, "Movement performance of human-robot cooperation control based on emg-driven hill-type and proportional models for an ankle power-assist exoskeleton robot," *IEEE Transactions on Neural Systems and Rehabilitation Engineering*, vol. 25, no. 8, pp. 1125–1134, 2017.
- [9] U. H. Tang, R. Zügner, V. Lisovskaja, J. Karlsson, K. Hagberg, and R. Tranberg, "Comparison of plantar pressure in three types of insole given to patients with diabetes at risk of developing foot ulcers—a two-year, randomized trial," *Journal of clinical & translational endocrinology*, vol. 1, no. 4, pp. 121–132, 2014.
- [10] A. Tsukahara, Y. Hasegawa, K. Eguchi, and Y. Sankai, "Restoration of gait for spinal cord injury patients using hal with intention estimator for preferable swing speed," *IEEE Transactions on neural systems and rehabilitation engineering*, vol. 23, no. 2, pp. 308–318, 2014.
- [11] S. Qiu, W. Guo, D. Caldwell, and F. Chen, "Exoskeleton online learning and estimation of human walking intention based on dynamical movement primitives," *IEEE Transactions on Cognitive and Developmental Systems*, pp. 1–1, 2020.
- [12] A. Razak, A. Hadi, A. Zayegh, R. K. Begg, and Y. Wahab, "Foot plantar pressure measurement system: A review," *Sensors*, vol. 12, no. 7, pp. 9884–9912, 2012.
- [13] Y. Ding, I. Galiana, A. T. Asbeck, S. M. M. De Rossi, J. Bae, T. R. T. Santos, V. L. de Araujo, S. Lee, K. G. Holt, and C. Walsh, "Biomechanical and physiological evaluation of multi-joint assistance with soft exosuits," *IEEE Transactions on Neural Systems and Rehabilitation Engineering*, vol. 25, no. 2, pp. 119–130, Feb 2017.
- [14] J. Zhang, C. C. Cheah, and S. H. Collins, "Experimental comparison of torque control methods on an ankle exoskeleton during human walking," in *2015 IEEE International Conference on Robotics and Automation (ICRA)*. IEEE, 2015, pp. 5584–5589.
- [15] K. Tanghe, F. De Groote, D. Lefeber, J. De Schutter, and E. Aertbeliën, "Gait trajectory and event prediction from state estimation for exoskeletons during gait," *IEEE Transactions on Neural Systems and Rehabilitation Engineering*, pp. 1–1, 2019.
- [16] V. R. Garate, A. Parri, T. Yan, M. Munih, R. M. Lova, N. Vitiello, and R. Ronsse, "Walking assistance using artificial primitives: a novel bioinspired framework using motor primitives for locomotion assistance through a wearable cooperative exoskeleton," *IEEE Robotics & Automation Magazine*, vol. 23, no. 1, pp. 83–95, 2016.
- [17] X. Wu, Y. Ma, X. Yong, C. Wang, Y. He, and N. Li, "Locomotion mode identification and gait phase estimation for exoskeletons during continuous multi-locomotion tasks," *IEEE Transactions on Cognitive and Developmental Systems*, pp. 1–1, 2019.
- [18] Y. Ding, M. Kim, S. Kuindersma, and C. J. Walsh, "Human-in-the-loop optimization of hip assistance with a soft exosuit during walking," *Science Robotics*, vol. 3, no. 15, p. eaar5438, 2018.
- [19] J. Zhang, P. Fiers, K. A. Witte, R. W. Jackson, K. L. Poggensee, C. G. Atkeson, and S. H. Collins, "Human-in-the-loop optimization of exoskeleton assistance during walking," *Science*, vol. 356, no. 6344, pp. 1280–1284, 2017.
- [20] H. Huang, F. Zhang, L. J. Hargrove, Z. Dou, D. R.

- Rogers, and K. B. Englehart, "Continuous locomotion-mode identification for prosthetic legs based on neuromuscular-mechanical fusion," *IEEE Transactions on Biomedical Engineering*, vol. 58, no. 10, pp. 2867–2875, 2011.
- [21] J. A. Brantley, T. P. Luu, S. Nakagome, and J. L. Contreras-Vidal, "Prediction of lower-limb joint kinematics from surface EMG during overground locomotion," in *2017 IEEE International Conference on Systems, Man, and Cybernetics (SMC)*. IEEE, 2017, pp. 1705–1709.
- [22] G. Durandau, D. Farina, and M. Sartori, "Robust real-time musculoskeletal modeling driven by electromyograms," *IEEE Transactions on Biomedical Engineering*, vol. 65, no. 3, pp. 556–564, March 2018.
- [23] H. Mannel, F. Marin, L. Claes, and L. Durselen, "Establishment of a knee-joint coordinate system from helical axes analysis—a kinematic approach without anatomical referencing," *IEEE Transactions on biomedical engineering*, vol. 51, no. 8, pp. 1341–1347, 2004.
- [24] A. G. Schache, R. Baker, and L. W. Lamoreux, "Defining the knee joint flexion–extension axis for purposes of quantitative gait analysis: an evaluation of methods," *Gait & Posture*, vol. 24, no. 1, pp. 100–109, 2006.
- [25] K. J. O'Donovan, R. Kamnik, D. T. O'Keeffe, and G. M. Lyons, "An inertial and magnetic sensor based technique for joint angle measurement," *Journal of biomechanics*, vol. 40, no. 12, pp. 2604–2611, 2007.
- [26] H. Zhou and H. Hu, "Reducing drifts in the inertial measurements of wrist and elbow positions," *IEEE Transactions on Instrumentation and Measurement*, vol. 59, no. 3, pp. 575–585, 2010.
- [27] Y. Tao, H. Hu, and H. Zhou, "Integration of vision and inertial sensors for 3d arm motion tracking in home-based rehabilitation," *The International Journal of Robotics Research*, vol. 26, no. 6, pp. 607–624, 2007.
- [28] T. Seel, J. Raisch, and T. Schauer, "Imu-based joint angle measurement for gait analysis," *Sensors*, vol. 14, no. 4, pp. 6891–6909, 2014.
- [29] D. Nowka, M. Kok, and T. Seel, "On motions that allow for identification of hinge joint axes from kinematic constraints and 6d imu data," in *2019 18th European Control Conference (ECC)*. IEEE, 2019, pp. 4325–4331.
- [30] L. Ren, R. K. Jones, and D. Howard, "Whole body inverse dynamics over a complete gait cycle based only on measured kinematics," *Journal of biomechanics*, vol. 41, no. 12, pp. 2750–2759, 2008.
- [31] A. Karatsidis, G. Bellusci, M. Schepers, M. De Zee, M. S. Andersen, and P. H. Veltink, "Net knee moment estimation using exclusively inertial measurement units," in *XXVI Congress of the International Society of Biomechanics*, 2017.
- [32] M. McGrath, D. Howard, and R. Baker, "A lagrange-based generalised formulation for the equations of motion of simple walking models," *Journal of biomechanics*, vol. 55, pp. 139–143, 2017.
- [33] W. R. Johnson, J. Alderson, D. Lloyd, and A. Mian, "Predicting athlete ground reaction forces and moments from spatio-temporal driven cnn models," *IEEE Transactions on Biomedical Engineering*, vol. 66, no. 3, pp. 689–694, 2018.
- [34] E. Shahabpoor, A. Pavic, J. M. Brownjohn, S. A. Billings, L.-z. Guo, and M. Bocian, "Real-life measurement of tri-axial walking ground reaction forces using optimal network of wearable inertial measurement units," *IEEE Transactions on Neural Systems and Rehabilitation Engineering*, vol. 26, no. 6, pp. 1243–1253, 2018.
- [35] G. Serrancolí, A. Falisse, C. Dembia, J. Vantilt, K. Tanghe, D. Lefeber, I. Jonkers, J. De Schutter, and F. De Groote, "Subject-exoskeleton contact model calibration leads to accurate interaction force predictions," *IEEE Transactions on Neural Systems and Rehabilitation Engineering*, vol. 27, no. 8, pp. 1597–1605, 2019.
- [36] J. Vantilt, C. Girardi, E. Aertbeliën, F. De Groote, and J. De Schutter, "Estimating contact forces and moments for walking robots and exoskeletons using complementary energy methods," *IEEE Robotics and Automation Letters*, vol. 3, no. 4, pp. 3410–3417, 2018.
- [37] A. Karatsidis, G. Bellusci, H. M. Schepers, M. De Zee, M. S. Andersen, and P. H. Veltink, "Estimation of ground reaction forces and moments during gait using only inertial motion capture," *Sensors*, vol. 17, no. 1, p. 75, 2017.
- [38] P. De Leva, "Adjustments to zatsiorsky-seluyanov" s segment inertia parameters," *J biomech*, vol. 29, no. 9, pp. 1223–1230, 1996.
- [39] D. A. Winter, *Biomechanics and motor control of human movement*. John Wiley & Sons, 2009.
- [40] D. Winter, "Biomechanical motor patterns in normal walking," *Journal of motor behavior*, vol. 15, no. 4, pp. 302–330, 1983.
- [41] B. J. Stetter, F. C. Krafft, S. Ringhof, T. Stein, and S. Sell, "A machine learning and wearable sensor based approach to estimate external knee flexion and adduction moments during various locomotion tasks," *Frontiers in Bioengineering and Biotechnology*, vol. 8, p. 9, 2020.
- [42] M. P. McGrath, *Appropriately complex modelling of healthy human walking*. University of Salford (United Kingdom), 2014.